Monitoring deforestation, forest health, and environmental criticality in a protected area periphery using Geospatial Techniques

Neel Chaminda Withanage[1,2], Prabuddh Kumar Mishra[3], Kamal Abdelrahman[4] and Rajender Singh[3]

[1] School of Geographical Science, Southwest University, Beibei District, Chongqing, PR China, China
[2] Department of Geography, Faculty of Humanities and Social Sciences, University of Ruhuna, Wellamadama, Matara, Sri Lanka
[3] Department of Geography, Shivaji College, University of Delhi, New Delhi, Delhi, India
[4] Department of Geology and Geophysics, King Saud University, Riyadh, Saudi Arabia

ABSTRACT

Protected areas in South Asia face significant challenges due to human disturbance and deforestation. The ongoing debate surrounds the recent surge in illegal encroachment of forest buffer zones in the Musali divisional secretariat division (DSD), which has led to a significant loss of forest cover over the past three decades. In this context, detecting changes in forest cover, assessing forest health, and evaluating environmental quality are crucial for sustainable forest management. As such, our efforts focused on assessing forest cover dynamics, forest health, and environmental conditions in the DSD from 1988 to 2022. We employed standardized image processing techniques, utilizing Landsat-5 (TM) and Landsat-8 (OLI) images. However, the forest area in the DSD has shown minimal changes, and environmental conditions and forest health have illustrated considerable spatial-temporal variations over the 34 years. The results indicated that 8.5 km^2 (1.9%) of forest cover in the DSD has been converted to other land use classes. Overall, the Normalized Difference Vegetation Index (NDVI) has declined over time, while Land Surface Temperature (LST) exhibits an increasing trend. The regression results demonstrated a robust inverse relationship between LST and NDVI. The declining vegetation conditions and the increasing LST contribute to an increase in environmental criticality. The derived maps and indices will be beneficial for forest authorities in identifying highly sensitive locations. Additionally, they could enable land use planners to develop sustainable land management strategies.

Subjects Ecology, Environmental Impacts, Forestry, Spatial and Geographic Information Science, Environmental Health
Keywords Deforestation, Environmental criticality index, Forest health, Land use, NDVI, Vegetation condition index

Submitted 3 March 2024
Accepted 18 June 2024
Published 18 July 2024

Corresponding author
Prabuddh Kumar Mishra,
prab19@gmail.com,
prabuddh@shivaji.du.ac.in

Academic editor
Clement Kent

Additional Information and Declarations can be found on page 22

DOI **10.7717/peerj.17714**

INTRODUCTION

Changes in land use/land cover (LULC) reflect the impacts of socioeconomic factors on the environment and human–environment interactions (*Kayet & Pathak, 2015*; *Wijesinghe & Withanage, 2021*; *Withanage, Mishra & Jayasinghe, 2024*). Thus, updated and reliable

land information is crucial for both current and future land use planning (*Wijesinghe & Withanage, 2021*). Employing multi-temporal satellite imagery for LULC change detection helps in comprehending landscape dynamics (*Rawat & Kumar, 2015*). Previous studies have indicated that LULC changes have resulted in significant damage to forest cover, leading to a rapid pace of deforestation. The growing population, urbanization, and infrastructure development have contributed to an imbalance between the supply and demand for forest products, posing a threat to forest ecosystems (*Koellner et al., 2008*). Deforestation has led to the disappearance of 420 million hectares of forest between 1990 and 2020 (*FAO, 2022* and *FAO, 2014*). The recent emphasis on non-consumptive use of forests has garnered the attention of forest conservation authorities worldwide, leading to sustainable forest management (*Ranagalage et al., 2020*). Reliable quantification of forest cover and vegetation health is essential for developing comprehensive forest resource management guidelines.

Changes in forest cover play a significant role in influencing LST, which in turn can directly impact energy balance, evapotranspiration, and precipitation patterns, ultimately altering vegetation conditions (*Jaafar et al., 2020*; *Deng et al., 2018*; *Culf et al., 1996*). Given the challenges associated with in-situ observations, sensor platforms can be employed to retrieve LST effectively (*Jaafar et al., 2020*). Numerous studies have utilized Landsat data to analyze forest cover dynamics and health, often by analyzing NDVI (*Jaafar et al., 2020*; *Culf et al., 1996*; *Deng et al., 2018*; *Malik, Shukla & Mishra, 2019*; *Jenerette et al., 2006*). The NDVI is a basic index used to assess vegetation cover, vegetation health, and photosynthetic activity and some studies implied that NDVI is an indicator of the link between LST and vegetation conditions (*Jaafar et al., 2020*; *Anbazhagan & Paramasivam, 2016*; *Peng et al., 2014*; *Yuan et al., 2017*). Additionally, it can be used as a proxy for biomass accumulation (*Jaafar et al., 2020*). NDVI is used to create other indices, such as the Vegetation Condition Index (VCI), by normalizing long-term satellite-based NDVI data (*Yin et al., 2024*). Moreover, LST and NDVI serve as indicators of changing environmental quality. The Environmental Criticality Index (ECI) is calculated based on the ratio between LST and NDVI by normalizing each layer. Accordingly, previous researchers have employed the ECI to assess varying levels of risk associated with environmental conditions (*Senanayake, Welivitiya & Nadeeka, 2013*; *Ranagalage, Estoque & Murayama, 2017*; *Saputra, Jamadi & Sari, 2023*).

While there have been numerous studies quantifying forest cover using remote sensing data in other areas (*Wickramagamage, 1998*; *Fernando & Edirisuriya, 2016*; *Ranagalage et al., 2020*), it is challenging to find similar studies in our study area. Therefore, our study fills this gap by measuring forest cover dynamics and evaluating forest health and environmental conditions between 1988 and 2022 in Musali DSD which located in the northern periphery of Vilpattu National Park, Sri Lanka. The study objective was to assess changes in forest cover, vegetation health, and environmental conditions using the Landsat time series dataset. Three standardized indices: LST; NDVI; and VCI, were employed to evaluate changes in forest health. Additionally, environmental condition was analyzed using the ECI.

MATERIALS AND METHODS

Study area

Musali is one of the five DSD located in the Mannar district of northwestern Sri Lanka. This DSD located within latitudes 8°31′26″N, 8°49′2″N and longitudes 8°3′2″E, 79°56′29″E. Nanaddan DSD bounds it to the North, while to the South lie the Anauradhapura and Puttalam districts. The Madu DSD marks its Eastern border, with the Gulf of Mannar stretching along its Western edge (Fig. 1). The total extent of the DSD is 475 Km^2 with 20 *Grama Niladhari Divisions* (GNDs). The population of the DSD is comparatively low and there was 29,011 population in 2021 with showing density is as 61 persons per km^2 (*Department of Census and Statistics, 2022*). The primary livelihood activities in the DSD include agriculture, fishing, and animal husbandry.

While the annual and monthly average rainfall for Sri Lanka stands at 2,397 mm and 200 mm respectively, the Musali experiences an annual average rainfall of 960 mm, with monthly averages ranging from 74 mm to 134 mm. Thus, DSD is characterized as one of the driest regions in Sri Lanka, with evapotranspiration reaching 2,135 mm/year, placing it within a semi-arid climate zone (*Athauda et al., 2024*). The average humidity in the DSD is approximately 75%, attributed to its location within the semi-arid zone. The DSD typically encountering only the tail end of the northeastern monsoon. In April, aside from the monsoon, the DSD also experiences rainfall from conventional rains. For the remainder of the year, DSD experiences a long dry season (*Land Use Policy Planning Department, 2016*). The rainfall pattern is very different from the southwestern side of Sri Lanka. The annual minimum temperature in DSD is 26 °C while annual maximum temperature is 35 °C (*Department of Census and Statistics, 2022*). There is little variation in the temperature during the entire year. The dry season is possibly the longest in Sri Lanka, and a brief and light monsoon season during the winter months. Agro-ecologically, the DSD falls into the low-country dry zone-DL3 (*Land Use Policy Planning Department, 2016*).

Most areas in DSD is comprised of lowlands (elevation: 0 to 12 m) with some scattered undulating surface topography (slope: 0° to 5°). The predominant geological formation comprises Miocene limestone and Quaternary deposits. The soil types in the area encompass yellow-brown sands, dune and beach sands, as well as lagoonal deposits (*Athauda et al., 2024*). Along the coastal area, sandy soils (Regosols) predominate, while saline and marshy lands are prevalent in the low-lying areas (*Land Use Policy Planning Department, 2016*). Various forest and vegetation types can be identified in the DSD, encompassing dry monsoon forest, riverine dry forest, mangroves, and dense forest.

Materials

The study primarily used Landsat-5 Thematic Mapper (TM) and Landsat-8 Operational Land Imager (OLI) multispectral image series to investigate the spatial and temporal variations in vegetation cover, vegetation health, and environmental conditions (*United State Geological survey, 2023*). All images were taken during the dry period of the southwest monsoon (February and August) with less than 5% cloud cover, sourced from the USGS Earth Explorer (https://earthexplorer.usgs.gov/) for the year 1988, 1996, 2009 and 2022. Table S1 summarizes the Landsat data specifications used for deriving LST, NDVI, ECI,

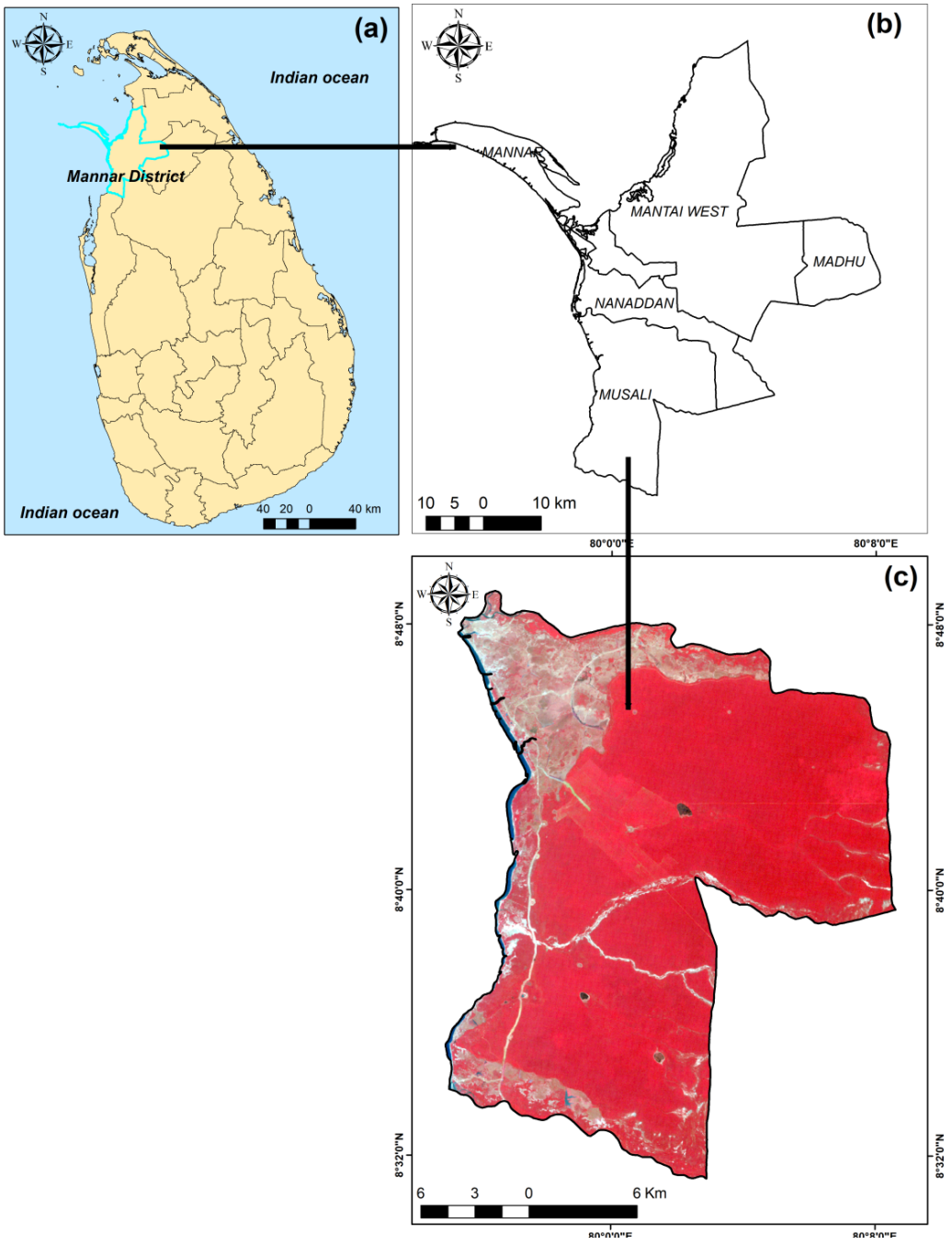

Figure 1 Location: (A) Sri Lanka; (B) DSD in Mannar district; (C) Landsat 4,3,2 composite of Musali DSD. Maps were created by authors using United States Geological Survey Earth Explorer Landsat images (https://earthexplorer.usgs.gov/) and Sri Lanka Survey department hard copy maps of DSD and Sri Lankan boundary.

Full-size DOI: 10.7717/peerj.17714/fig-1

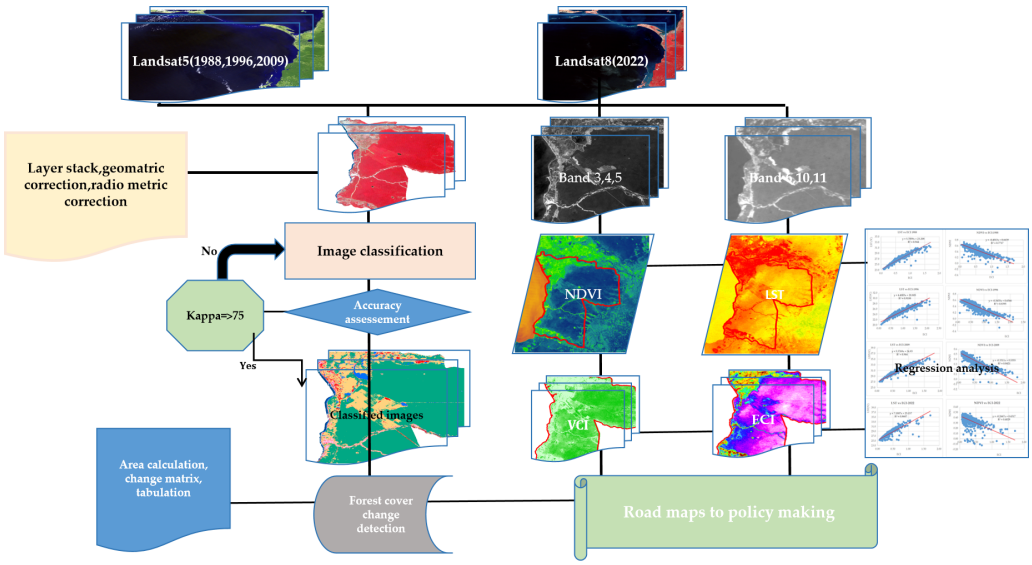

Figure 2 Methodological flowchart of the study. Maps were created by authors using United States Geological Survey Earth Explorer Landsat images (https://earthexplorer.usgs.gov/) and Sri Lanka Survey department hard copy maps of DSD and Sri Lankan boundary.

Full-size DOI: 10.7717/peerj.17714/fig-2

and for mapping forest cover changes. To create the study area boundary map and the Sri Lanka boundary map, hard copy maps available for purchase from the Sri Lanka Survey Department were used. ArcMap 10.8 software (ESRI, February, 2020) was used for remote sensing image processing, while regression analysis was performed using MS Office Excel (2013) spreadsheet program.

Methods

Several steps were followed to create forest cover maps and other indices, including image pre processing, classification, accuracy assessment, change detection, and the calculation of NDVI, LST, VCI, and ECI. Finally, regression analysis was performed to find the correlation between NDVI and LST for the concerned period. The methodical flowchart is represented in Fig. 2.

Image pre processing

Pre processing of data involved several key steps to ensure that the data is clean, accurate, and ready for analysis. Firstly, radiometric calibration was performed by converting raw digital numbers (DN) to radiance or reflectance values. This process corrected sensor-specific biases. Secondly, we removed the effects of the atmosphere on the reflectance values by employing Dark Object Subtraction (DOS). To maintain spatial consistency, we performed geometric correction by projecting all data layers into the WGS 1984, UTM zone 44N projection system. In the image subsetting phase, we clipped the images to the areas of interest (AOI) using the DSD boundary. Then, we adjusted the spatial resolution of the Landsat images using the nearest neighbor resampling technique while maintaining a 30 m spatial resolution.

Image classification

The features in the images were retrieved to predetermine the forest cover changes in Musali DSD. During classification, five land use classes were identified: forest, agriculture, water bodies, built-up/settlements, and others, as shown in Table S2. There are various statistically driven supervised classification algorithms, such as maximum likelihood, parallelepiped, and Mahalanobis. The chosen classification method for this study is maximum likelihood classification (MLC). MLC, a widely used algorithm for LULC classification, relies on statistical sampling using probability density functions to detect predefined sets of LULC classes (*Alawamy et al., 2020*). Moreover, this method is widely used because fine-resolution satellite remote sensing data are comparatively inexpensive sources for LULC mapping (*Weng, 2002*; *Dissanayake et al., 2019*). It relies upon the likelihood that a pixel belongs to a specific class. One well-known method, MLC, based on the Bayesian equation, calculates the likelihood D of unknown measurement vector X, belongs to Eq. (1) (*Mohajane et al., 2018*):

$$D = \ln(a_c) - [0.5 \ln(|Cov_c|)] - [0.5\{X - M_c)T(Cov_c - 1)(XM_c)] \quad (1)$$

In the equation the weighted distance represent by D; particular class is c; the measurement vector of the candidate pixel is represented by X. The mean vector of the sample of class c represented by M_c. The percent probability of the candidate pixel being a member of class c represented by a_c. The covariance matrix of the pixels in the sample of class c is presented by Cov_c. $|Cov_c|$ is the determinant of Cov_c (matrix algebra). $Cov_c - 1$ is is the inverse of Cov_c (matrix algebra). ln = natural logarithm function; and T = transposition function (matrix algebra) (*Mohajane et al., 2018*).

The majority filtering method has been employed to rectify the errors that may arise during the classification process. This approach has been utilized by previous researchers as well to bolster the reliability of their results (*Weng, 2002*; *Dissanayake et al., 2019*). Figure S1 illustrates the LULC information provided in Table S2. These images were collected from the Google Earth Pro. August 25, 2022, was the date for selecting the images as it is the closest available date to offer an illustrative representation of the LULC information.

Accuracy assessment

Securing the quality of classified images is paramount in every LULC change detection process. To achieve this, a stratified random sampling technique was employed in the procedure, ensuring coverage of all LULC classes, with 600 Ground Control Points (GCP) created each year (*Wu & Murray, 2003*). Subsequently, Google Earth Pro historical imagery served as reference data for accuracy assessment. Four widely used accuracy metrics were computed: Overall Accuracy (OA), Producer's Accuracy (PA), User's Accuracy (UA), and Kappa Coefficients (K).

OA represents the overall percentage of correctly classified LULC classes, calculated by dividing the number of accurately classified land cover pixels by the total number of pixels in the datasets using Eq. (2) (*Yuh et al., 2023*; *Olofsson et al., 2014*; *Weng, 2002*;

Dissanayake et al., 2019; *Estoque & Murayama, 2017*).

$$OA = \frac{1}{N}\sum_{ii=1}^{n} P_{ii} \tag{2}$$

where, OA is overall accuracy; N is total samples number; n is total categories number; and Pii is correct classifications number of ith sample in confusion matrix.

PA measures the percentage accuracy of individual LULC classes within a map, determined by dividing the number of correctly classified pixels in a specific land cover class by the total number of pixels belonging to that class in the reference data. Misclassified pixels within this metric are known as errors of omission and was calculated using as Eq. (3):

$$PA = \frac{\text{Correctly classified number pixel in each category}}{\text{Correctly classified total number pixels in that category (column total)}} \tag{3}$$

UA evaluates the reliability of a given land cover map concerning its agreement with ground observations. It is calculated by dividing the number of correctly classified pixels in a specific land cover class by the total number of pixels classified within that class. Similar to Producer's Accuracy, misclassified pixels in this metric are referred to as errors of omission. Equation (4) is as below:

$$UA = \frac{\text{Correctly classified number pixel in each category}}{\text{Correctly classified total number pixels in that category(row total)}} \tag{4}$$

K indicates the level of agreement between test and validation data in a generated land cover map. It is based on the probability of the test data closely matching the validation data during the land cover mapping process and is highly correlated with overall accuracy. K coefficient was utilized as a metric to gauge the agreement between classified results and actual conditions, thereby determining the levels of accuracy. A threshold of 0.75 or higher was set, indicating sufficient agreement for actionable insights based on the image. The Eq. (5) was used to calculate the K (*Alqurashi & Kumar, 2014*). The results of the accuracy assessments are presented in Table S3.

$$K = \frac{N\sum_{i=j}^{k} x_{ii} - \sum_{i=1}^{k}(x_{i+} \times x_{+i})}{N^2 - \sum_{i=1}^{k}(x_{i+} \times x_{+i})} \tag{5}$$

where k is the number of rows in the matrix; x_{ii} is the number of observations in row i and column i; x_i+ and $x+_i$ are the marginal totals of row k and column i. N is the number of observations (*Alqurashi & Kumar, 2014*).

Change detection

A change detection method was used to cross-tabulate LULC data between different periods after image classification: (i) 1988 *vs.* 1996, (ii) 1996 *vs.* 2009, (iii) 2009 *vs.* 2022, and (iv) 1988 *vs.* 2022.

Retrieval of LST

LST is commonly defined as the temperature at the interface between the Earth's surface and its atmosphere and this serves as a critical indicator in all physical processes concerning

surface energy and water balance at both micro and macro spatial scale (*Malik, Shukla & Mishra, 2019*; *Sobrino, Jiménez-Muñoz & Paolini, 2004*). This plays a pivotal role in surface processes and boasts a wide array of applications, including vegetation stress monitoring, climate change studies, environmental assessment, and urban climate analysis. With the availability of large-scale remote sensing data, near-surface air temperature measurements can be effectively monitored and utilized to retrieve the temperature of various LULC surfaces (*Malik, Shukla & Mishra, 2019*). In our study, Landsat 5 and Landsat 8 data were employed to analyze LST and investigate the impact of forest degradation. The LST was obtained by Thermal Infrared (TIR) band 6 of Landsat 5 and TIR band 10 and 11 of Landsat 8 by converting DN values into radiance values (*Jaafar et al., 2020*; *Ranagalage, Estoque & Murayama, 2017*; *Dissanayake et al., 2019*). Here we used thremal bands holding brightness temperatures which are represented in Kelvin. Before retrieval, the LST land surface emissivity values was derived using Eq. (6):

$$\varepsilon = mP_{\mathrm{V}} + n \tag{6}$$

where ε represents land surface emissivity; m represents $(\varepsilon_v - \varepsilon_s) - (1 - \varepsilon_s)\,\varepsilon_v$; P_v represents the amount of vegetation; n represents $\varepsilon_s + (1 - \varepsilon_s)\,\varepsilon_v$; ε_s is soil emissivity; ε_v is the vegetation emissivity; and F is a shape factor (*Ranagalage, Estoque & Murayama, 2017*; *Dissanayake et al., 2019*). Here we used $m = 0.004$ and $n = 0.986$ as in previous research (*Jaafar et al., 2020*; *Ranagalage, Estoque & Murayama, 2017*; *Dissanayake et al., 2019*). The proportion of vegetation (PV) is derived from Eq. (7).

$$\mathrm{PV} = ((\mathrm{NDVI} - \mathrm{NDVImin})/(\mathrm{NDVImax} - \mathrm{NDVImin}))^2 \tag{7}$$

where NDVI is the normalized difference vegetation index derived from Eq. (9) as in sub section below. The NDVImin and NDVImax are the minimum and maximum values of the NDVI, respectively. Then emissivity corrected LST were retrieved using Eq. (8).

$$LST\left(^{\circ}C\right) = \frac{TB}{1} + (\lambda \times TB/p)In\varepsilon \tag{8}$$

where TB = Landsat TM Band 6 at-satellite brightness temperature; λ = wavelength of emitted radiance (λ = 11.5 μm for Landsat TM Band 6, λ = 10.8 μm for Landsat TIRS Band 10) (*Ranagalage, Estoque & Murayama, 2017*; *Dissanayake et al., 2019*); p = h × c/σ(1. 438× 10 −2 mK), σ = Boltzmann constant (1. 38 × 10− 23 J/K), h = Planck's constant (6. 626 × 10− 34 Js),c = velocity of light (2. 998× 108 m/s), ε is the land surface emissivity. Last, the LST values of Kelvin were converted into degrees Celsius (°C).

Derivation of NDVI

The results of spectral analysis are typically summarized into vegetation indices, which establish relationships between reflectance across two or more wavelength intervals or bands in satellite images. Measurement of such indices serves as an especially valuable tool for precision agriculture and vegetation analysis (*Fernández-Alonso, Hernández & Torres-Costa, 2023*). Various sensors and multi spectral devices are extensively utilized nowadays to assess the condition of vegetation, including chlorophyll meters, canopy reflectance sensors, and Plant-O-Meter (*Padilla et al., 2018*; *Kitić et al., 2019*). NDVI is the

most common vegetation index, frequently employed as an indicator of chlorophyll content and overall vegetation health (*Fernández-Alonso, Hernández & Torres-Costa, 2023*). The NDVI is a vital remote sensing metric, acting as a key indicator for assessing vegetation coverage and growth. This quantifies vegetation through the spectral reflectance and derived from the ratio of the difference to the sum of values in the red and near-infrared bands, with values typically ranging from −1.0 to 1.0 (*Yin et al., 2024*). Near infrared (NIR) (band 4 in TM and band 5 in OLI) and red bands (band 3 in TM and band 4 in OLI) of Landsat are needed to retrieve the NDVI. Vegetation density and chlorophyll activity variations were measured using the Landsat images which were taken during the dry period of the study area using Eq. (9) (*Jaafar et al., 2020*; *Ranagalage, Estoque & Murayama, 2017*; *Dissanayake et al., 2019*).

$$\mathrm{NDVI} = (\mathrm{NIR} - \mathrm{RED})/(\mathrm{NIR} + \mathrm{RED}) \tag{9}$$

The retrieved maps were classified upon their values.We used the thresholding method to classify NDVI into four categories: non vegetation (less than 0) low-density vegetation (0–0.2), moderate-density vegetation (values between 0.2 and 0.5), and high-density vegetation (values above 0.5) following the similar work conducted by *Mohajane et al. (2018)*.

Derivation of VCI

VCI is a widely used drought index which developed by *Kogan (1990)* for monitoring vegetation drought stress and estimating drought trends. *Kogan (1990)* developed this index to enhance the weather-related components in the NDVI value (*Ha, Uereyen & Kuenzer, 2023*). It is constructed by normalizing long-term satellite-based NDVI data. The VCI offers several advantages, such as eliminating envelope signal variations in NDVI and accounting for regional climate diversity. It is also easy to construct using only NDVI data. Consequently, it has various applications, including drought investigation, crop yield estimation, and vegetation dynamics assessment (*Yin et al., 2024*; *Ha, Uereyen & Kuenzer, 2023*). This helps to compare current NDVI values with past year NDVI values of the same season. Equation (10) was used to calculate VCI for the selected years (*Yin et al., 2024*; *Ha, Uereyen & Kuenzer, 2023*; *Kogan, 1990*; *Dutta et al., 2015*).

$$\mathrm{VCI} = (\mathrm{NDVI} - \mathrm{NDVImin})/(\mathrm{NDVImax} - \mathrm{NDVImin}) * 100 \tag{10}$$

where NDVI indicates the value of a specific pixel in that particular month, NDVImax and NDVImin show the multi-layer highest and lowest NDVI values in the same period. The VCI values represented as % and 0 is for extreme drought conditions and 100 is optimal vegetation health. Following (*Ha, Uereyen & Kuenzer, 2023*; *Kogan, 1990*; *Dutta et al., 2015*), we classified VCI values into five categories upon drought severity: non drought (100%–50%), mild drought (50%–30%), moderate drought (30%–20%), severe drought (20%–10%), and extreme drought (less than 10%).

Derivation of ECI

Due to rising LST and declining NDVI, the environment is in a critical state, as measured by the ECI. Increases in LST have been shown to directly correlate with ECI, while decreases in

NDVI have been reported to have an inverse correlation with ECI (*Senanayake, Welivitiya & Nadeeka, 2013*; *Saputra, Jamadi & Sari, 2023*). Based on the ratio between LST and NDVI the ECI is calculated to identify environmentally critical areas (*Senanayake, Welivitiya & Nadeeka, 2013*; *Ranagalage, Estoque & Murayama, 2017*)). The LST and NDVI layers are used to derive the ECI using Eq. (11). The retrieved NDVI and LST layers were first normalized using the histogram equalization method, which ranges pixel values between 1–255 (*Ranagalage, Estoque & Murayama, 2017*). The higher the ECI value, the more environmentally critical. The spatial variation of ECI over the study area was interpreted as high, medium, and low.

$$\text{ECI} = \text{LST (Stretched } 1-255)/\text{NDVI (Stretched } 1-255). \quad (11)$$

RESULTS

Forest cover change in Musali DS

Figures 3 and 4 illustrate the spatial and temporal variations of the LULC in the study area. According to the findings presented in Table 1, the forest area has decreased from 348.7 km^2 (73.5%) to 340 km^2 (71.6%) over 34 years. The urban areas and settlements have expanded from 13.9 km^2 (2.9%) to 28 km^2 (5.8%) between 1988 and 2022, primarily driven by population growth and other socioeconomic factors. Agricultural lands have decreased by 2.2 km^2 over this period. The area of water bodies has diminished by approximately 2.4 km^2, while other land uses (sand and salt marshes) have decreased by approximately 1 km^2. Between 1988 and 1996, forest cover experienced a significant decrease, with a negative change of approximately −9.7 km^2 (Table 2). Consequently, the net change in forest area over the 34-year period is −8.09 km^2, reflecting a gain of 20.5 km^2 and a loss of 28.6 km^2. The primary cause of the decline in forest area is the expansion of agriculture and settlements, as depicted in Fig. S2.

Within the specified time frame, approximately 4.8 km^2 of forest land was converted into agricultural areas, specifically for paddy fields (Fig. S2). Additionally, a total of 2.75 km^2 of forest land was converted into built-up areas. Between 1988 and 1996, the majority of the scattered forest patches in the northwestern area (Fig. 5A) were converted into agricultural areas. Between 1996 and 2009, a significant portion of the forest lands adjacent to roadways, as seen in Figs. 5C and 5D, were taken over by human settlements and developed areas. Over time, a significant portion of agricultural land owned by Kondachchi Plantation Limited within Vilpattu National Park has been converted into forest areas (Fig. 5E). Between 2009 and 2022, forest areas along the northern boundary, southeastern, and eastern portions experienced conversion into agricultural and residential areas. Over 34 years, there has been a 3% expansion in built-up and settlement areas, totaling approximately 14.35 km^2. Additionally, there has been a reduction of forest cover by about 8.09 km^2.

Spatial-temporal changes of NDVI and LST

The spatial and temporal distribution of NDVI shows significant variability. Despite deforestation experiencing relatively minor changes over 34 years, the NDVI indicates

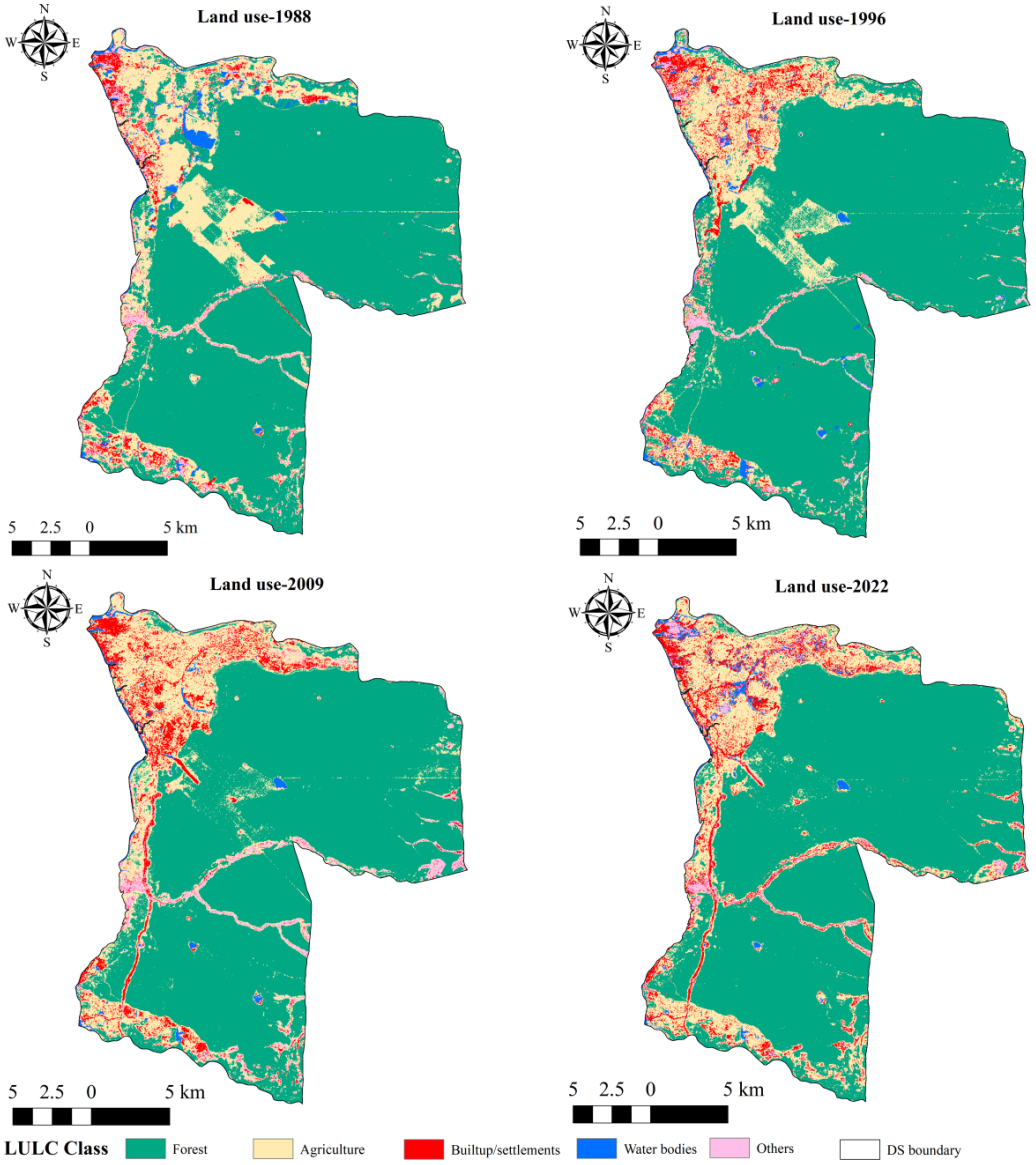

Figure 3 **Land use in Musali DSD: 1988; 1996; 2009; 2022.** Maps were created by authors using United States Geological Survey Earth Explorer Landsat images (https://earthexplorer.usgs.gov/) and Sri Lanka Survey department hard copy maps of DSD and Sri Lankan boundary.

Full-size DOI: 10.7717/peerj.17714/fig-3

a significant decline, suggesting a deterioration in the health of the vegetation in the region. The NDVI shows a significant reduction in high-density vegetation areas, which have transitioned into moderate- and low-density vegetation areas over the past 34 years. Additionally, there has been an increase in non-vegetation areas (Figs. 6A–6D). The corresponding descriptive statistics, as shown in Table S4, also support this phenomenon. In 1988, NDVI values ranged from −0.55 to 0.75, indicating extensive high-density vegetation coverage across the study area (Fig. 6A). However, in 2022, this range decreased from −0.18 to 0.54. At all four time points, areas with high NDVI values were found in

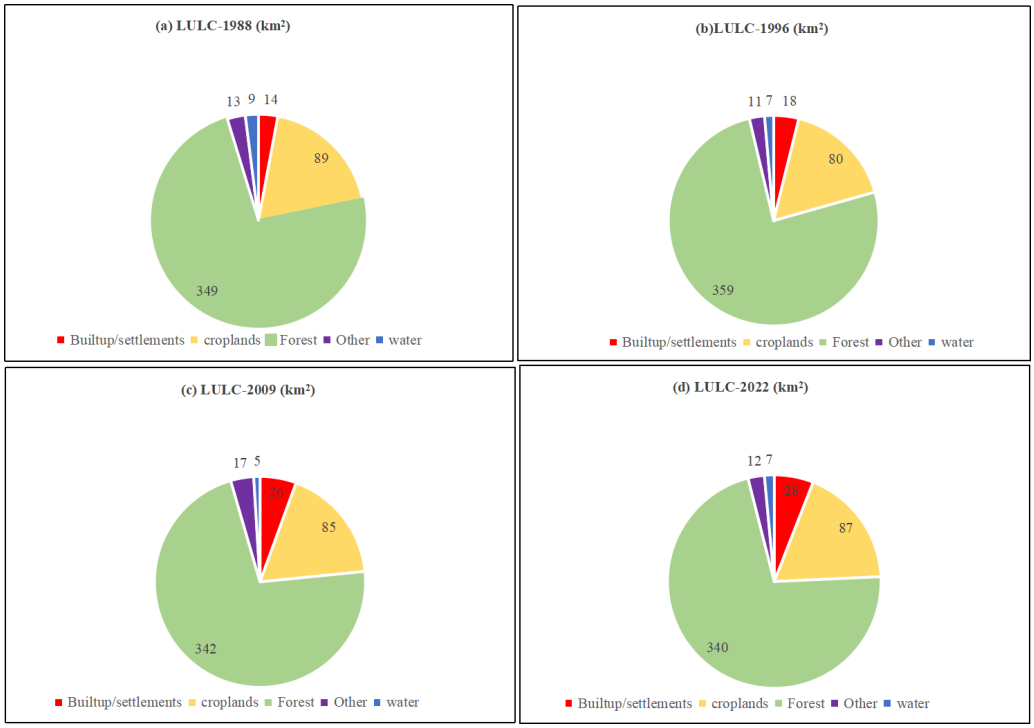

Figure 4 **Land use statistics in Musali DSD: (A) 1988; (B) 1996; (C) 2009; (D) 2022.**
Full-size DOI: 10.7717/peerj.17714/fig-4

Table 1 **LULC changes summary in Musali DSD,1988-2022.**

LULC	1988		1996		2009		2022	
	Area (km^2)	%	Area (km^2)	%	Area (km^2)	%	Area (km^2)	%
FC	348.72	73.5	345.56	72.4	342.05	72.01	340.2	71.6
AG	89.27	18.7	93.54	19.6	84.72	17.8	87.4	18.4
BS	13.95	2.9	18.28	3.8	26.39	5.5	28.3	5.9
WB	9.45	1.98	6.57	1.3	4.53	0.95	7.1	1.4
OT	13.05	2.74	11.05	2.3	16.74	3.5	12.0	2.5
Total	474.44	99.8	474.44	99.8	474.44	99.8	474.44	99.8

Notes.
FC, Forest cover; AG, Agriculture; BS, Built-up/settlements; WB, Water bodies; OT, Others.

high-density and moderate-density vegetation areas, while areas with low NDVI values were concentrated in non vegetation and settlement areas, as depicted in Fig. 6B. Between 1988 and 1996, the NDVI indicated a significant decrease in high-density vegetation in the study area while non-vegetation areas expanded (Figs. 6C, 6D). This trend continued further in 2009 and 2022. The areas of Silavatura, Alakaddu, and Putukulam, which have recently been developed and populated, have exhibited a decrease in NDVI values by the year 2022. The northern portion of the region features paddy fields with low NDVI values.

The spatial and temporal changes in LST over 34 years are depicted in Figs. 7A–7D. In 1988, the lowest recorded LST was 22.3 °C, while the highest recorded LST was 32.8 °C.

Table 2 Statistics of forest cover changes in Musali DSD.

	1988–1996	1996–2009	2009–2022	1988–2022
Forest gain (km^2)	14	11.7	6.3	20.5
Forest loss (km^2)	23.7	28.2	7.8	28.6
Net Change (+/-)	−9.7	−16.5	−1.5	−8.09

The average LST for that year was 25.2 °C. Nevertheless, the temperature has risen by approximately 6 °C by 2022, reaching a minimum of 24.5 °C and a maximum of 38.8 °C, with an average of 26 °C (Table S5). Areas that are not covered by forests exhibit elevated LST, particularly in built-up and residential areas. Specifically, in the year 2022, new residential areas and deforested areas in Marichchakattu, Kondachchi plantation, and Alakaddu are indicated as prominent hot spots in Fig. 7D. Nevertheless, the areas with high LST in the northern part experienced a significant decrease in LST by 2022 compared to the years 1988, 1996, and 2009. However, the LST in the areas that were deforested between 1988 and 1996 in the northern boundary showed a rise after 2009.

Figure 8 illustrates the regression results for the correlation between NDVI and LST for the years 1988, 1996, 2009, and 2022. The scatter plots demonstrate a strong inverse relationship between LST and NDVI across three time points. The coefficient of determination (R^2) values for the years 1988, 1996, and 2009 are indeed quite high. Furthermore, there was a noticeable upward trend in the data, indicating the strong predictive ability of NDVI in explaining the spatial changes in LST throughout the three time points, except for 2022 that shows the low R^2 value as 0.339.

Variation of VCI 1988–2022

Examination of the VCI values reveals notable spatial and temporal variations in vegetation health within the DSD across four periods. In 1988, the average VCI value stood at 93.4, yet it plummeted to a mean of 15.2 by 2022. Over the span of 34 years, the standard deviation has escalated from 17.7 to 31.8. Figure 9 depicts the spatial distribution trends of vegetation health at four distinct period. In 1988, vegetation health was good, as most areas of the DSD experienced non-drought or mild drought conditions (Fig. 9A). However, by 1996, vegetation stress had increased significantly due to extreme and severe drought conditions, particularly impacting the northwestern region (Fig. 9B). Although extreme and severe drought conditions were not as prevalent as in 1996, the areas experiencing non-drought and mild drought conditions had further decreased by 2009 (Fig. 9C). In 2022, the vegetation health shows an improvement compared to 2009, with non-drought vegetation coverage expanding once more, except in areas of extreme and severe drought in the northwestern region (Fig. 9D). This phenomenon can be ascribed to the favorable climatic conditions prevalent in year 2022. By 2022, there was a notable increase in vegetation stress observed in the northwestern and southern boundaries compared to the levels recorded in 2009.

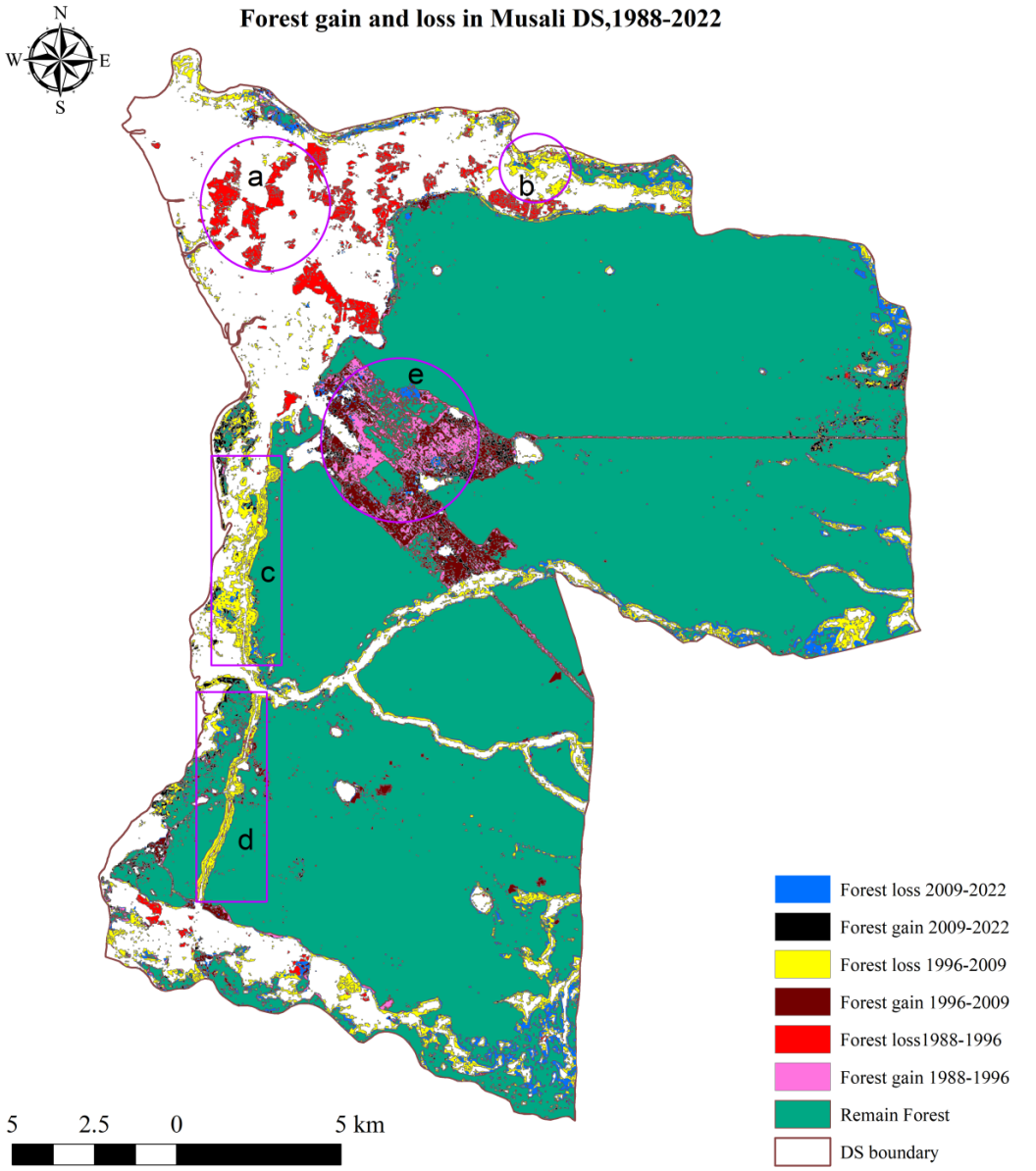

Figure 5 Forest cover change in Musali DSD: 1988; 1996; 2009; 2022. Maps were created by authors using United States Geological Survey Earth Explorer Landsat images (https://earthexplorer.usgs.gov/) and Sri Lanka Survey department hard copy maps of DSD and Sri Lankan boundary.

Full-size DOI: 10.7717/peerj.17714/fig-5

ECI in 1988, 1996, 2009, and 2022

Figures 10A–10D displays the ECI of the DSD for the years 1988, 1996, 2009, and 2022. The analysis reveals a steady increase in the ECI value by 2022. Initially recorded at 7.74 in 1988, the ECI has progressively climbed to 9.3, 12.8, and 15.5 in 1996, 2009, and 2022, respectively. According to the distribution maps, the areas with the highest ECI values were primarily situated within the settlements and built-up areas in the DS across all four time points. Generally, dense forested regions exhibiting low ECI values suggest minimal

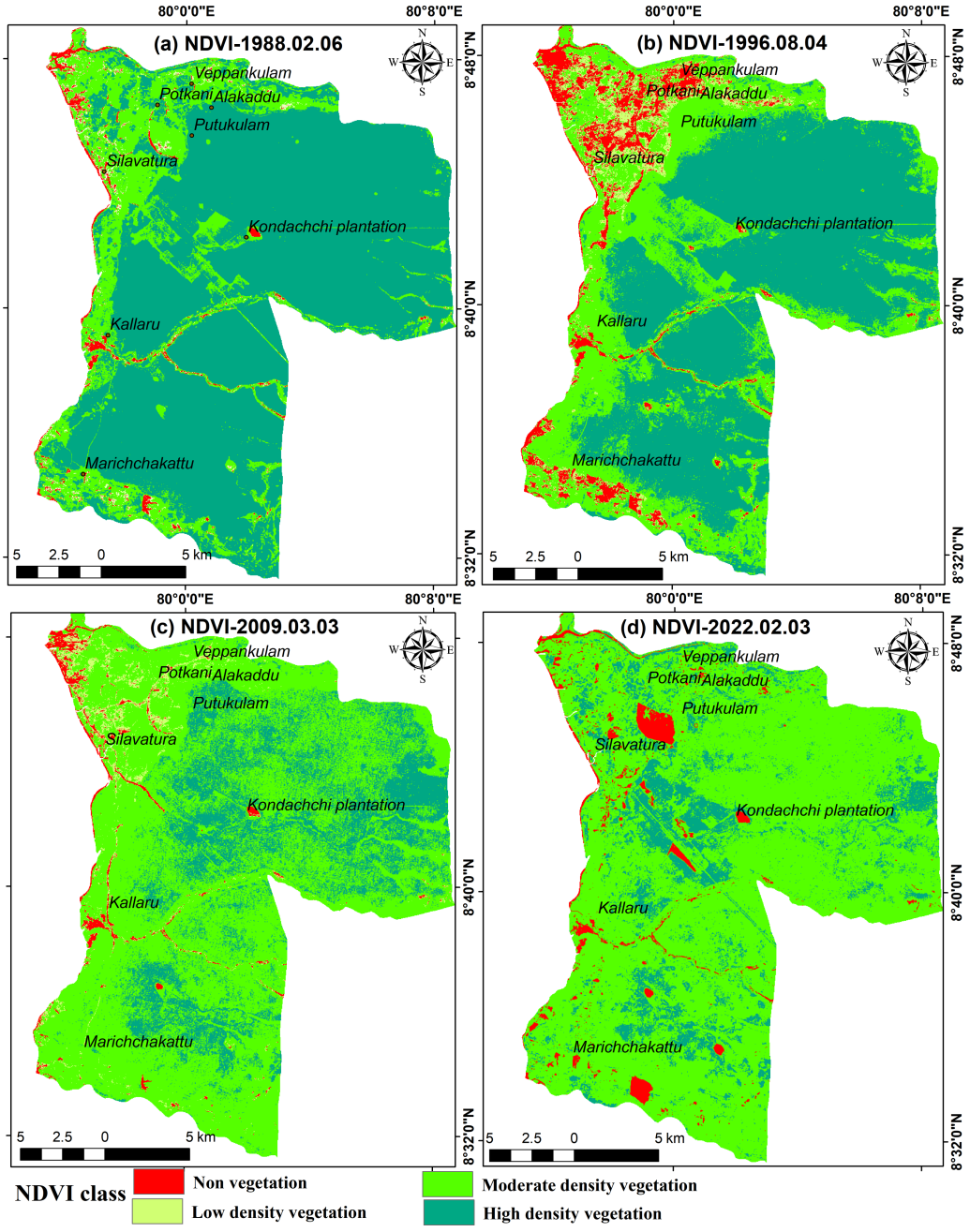

Figure 6 Spatial changes of NDVI in Musali DSD: (A) 1988; (B) 1996; (C) 2009; (D) 2022. Maps were created by authors using United States Geological Survey Earth Explorer Landsat images (https://earthexplorer.usgs.gov/) and Sri Lanka Survey department hard copy maps of DSD and Sri Lankan boundary.

Full-size DOI: 10.7717/peerj.17714/fig-6

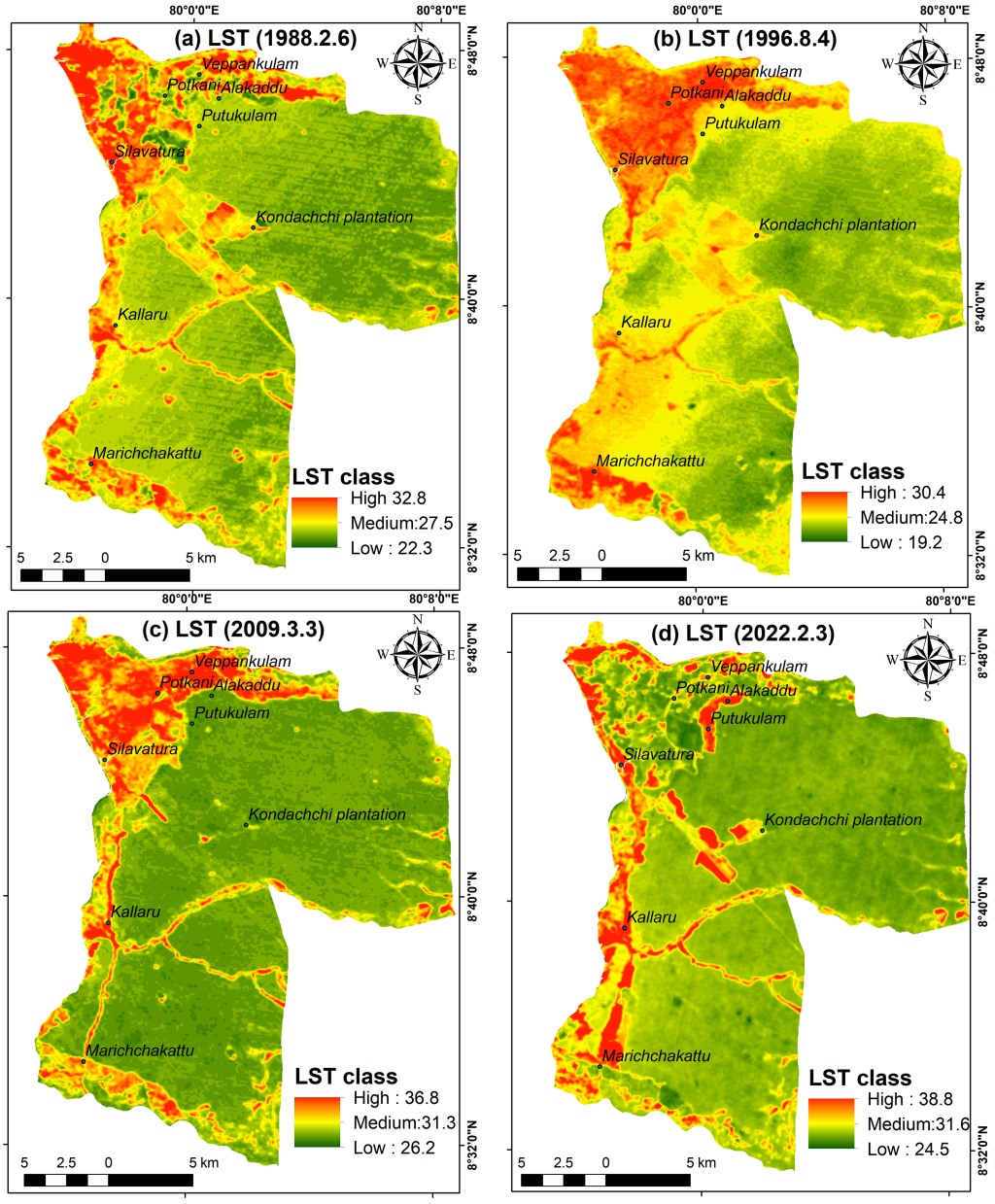

Figure 7 Spatial changes of LST in Musali DSD: (A) 1988; (B) 1996; (C) 2009; (D) 2022. Maps were created by authors using United States Geological Survey Earth Explorer Landsat images (https://earthexplorer.usgs.gov/) and Sri Lanka Survey department hard copy maps of DSD and Sri Lankan boundary.

Full-size DOI: 10.7717/peerj.17714/fig-7

impact on the ecosystem. However,built-up areas along the northwestern boundary, such as Arippu, consistently displayed a notable concentration of ECI values across all four time points, including 1988 (Fig. 9A). Moreover, new concentrations of ECI have emerged in recently deforested regions such as Marichchakattu, Alakaddu, and the Kondachchi plantation area, as illustrated in Fig. 9D.

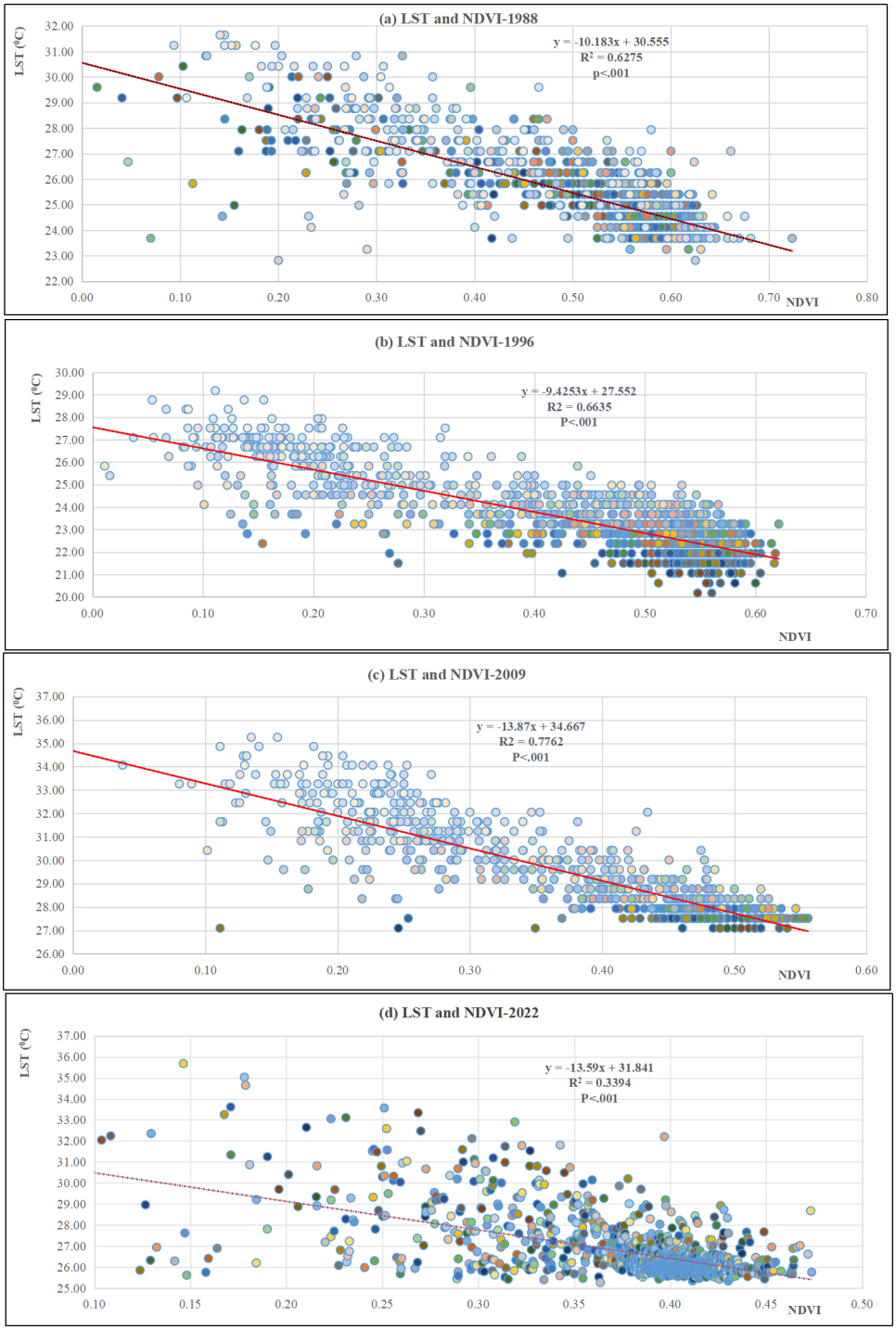

Figure 8 Regression results between NDVI and LST in Musali DSD: (A) 1988; (B) 1996; (C) 2009; (D) 2022.

Full-size DOI: 10.7717/peerj.17714/fig-8

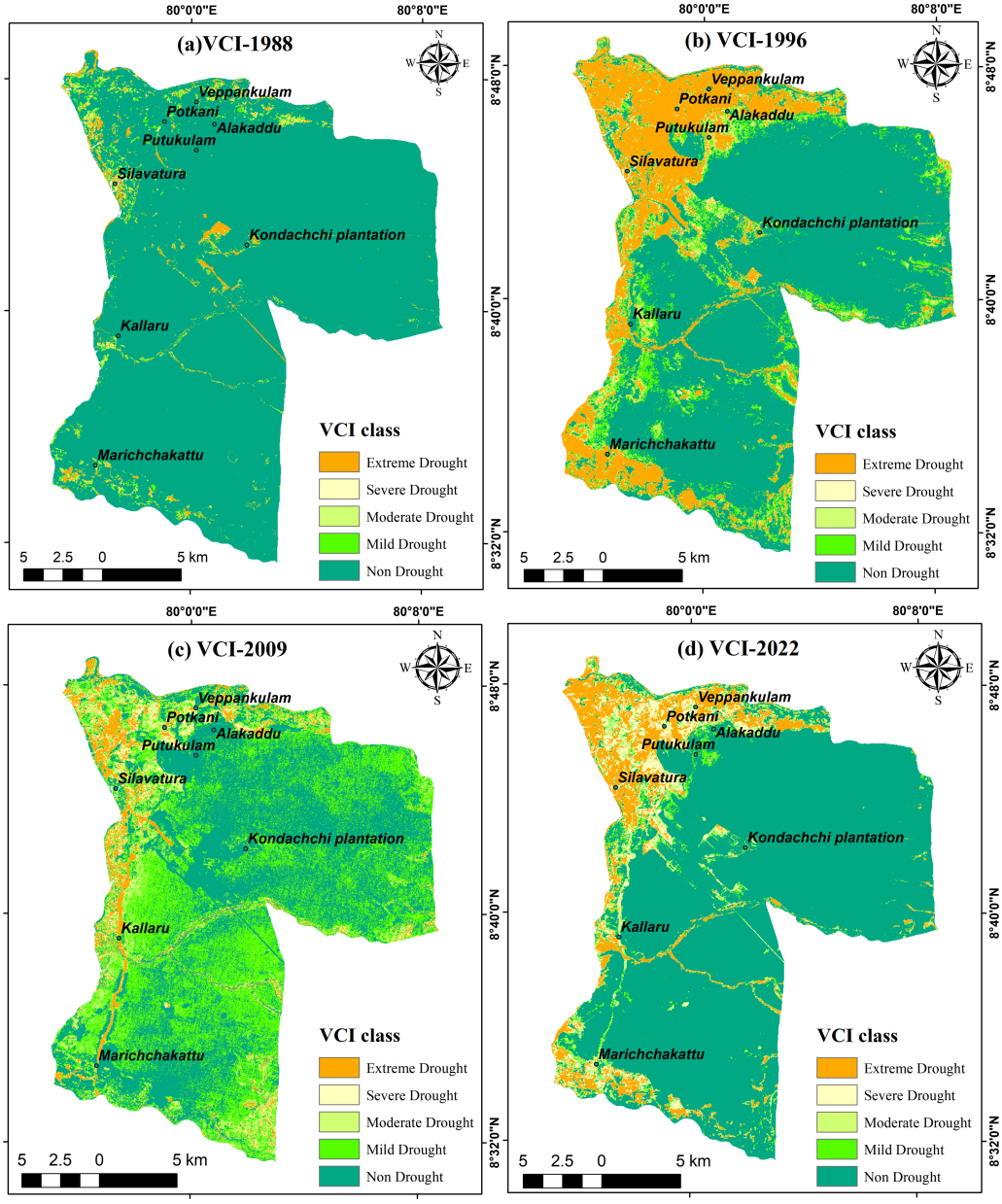

Figure 9 Vegetation Condition Index in DSD: (A) 1988; (B) 1996; (C) 2009; (D) 2022. Maps were created by authors using United States Geological Survey Earth Explorer Landsat images (https://earthexplorer.usgs.gov/) and Sri Lanka Survey department hard copy maps of DSD and Sri Lankan boundary.

Full-size DOI: 10.7717/peerj.17714/fig-9

DISCUSSION

The trends and Drivers of forest cover change

To sum up, our research indicates that over the course of 34 years, there has been a steady rate of deforestation occurring in an area adjacent to the northern boundary of the Vilpattu National Park. This deforestation appears to stem from the establishment and

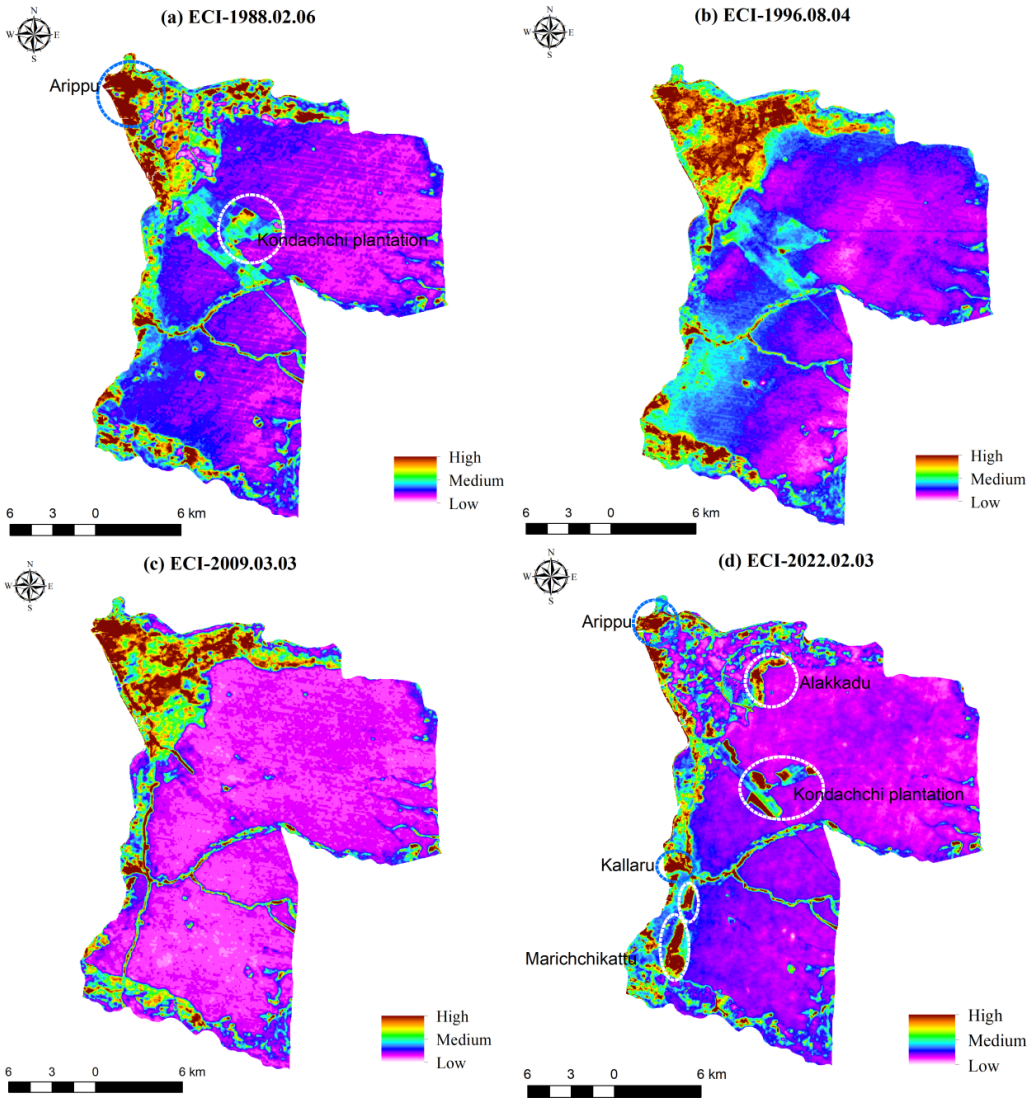

Figure 10 Environmental Criticality Index in DSD: (A) 1988; (B) 1996; (C) 2009; (D) 2022. Maps were created by authors using United States Geological Survey Earth Explorer Landsat images (https://earthexplorer.usgs.gov/) and Sri Lanka Survey department hard copy maps of DSD and Sri Lankan boundary.

Full-size DOI: 10.7717/peerj.17714/fig-10

expansion of human settlements in the vicinity. *Ranagalage et al. (2020)* also found that the deforestation rate in dry zone regions from 2009 to 2020 stood at 3.4%. The gradual pace of deforestation observed in the examined area could have influenced the dynamics of the civil conflict spanning from 1988 to 2009, potentially leading to fewer new settlements and limited expansion of agricultural lands. Furthermore, they found that the civil war resulted in swift forest regeneration across the northern and eastern province. This resurgence can be attributed to the abandonment of human settlements and other disruptions caused by *Chena* cultivation. Due to the civil war, a considerable portion of the population moved from the study area to different districts within the country. The main factors driving the

decline in forest cover in the study area after 2009 were resettlement efforts following the war, infrastructure development, and various rural development projects (*Fernando et al., 2015*; *Fernando & Edirisuriya, 2016*; *Wickramagamage, 1998*; *Forest Department Government of Sri Lanka, 2009*). *Rathnayake, Jones & Soto-Berelov (2020)* also observed that LULC changes have affected protected areas in Sri Lanka. They noted that many protected areas situated near district capitals have experienced significant impacts due to rising human population pressure and urbanization. Following 2009, a notable portion of the forested areas in the dry zone underwent conversion into settlements and agricultural lands. This transformation occurred as a result of the majority of displaced individuals returning to their native residences, leading to encroachments on the forest buffer zone within the study area (Fig. S3). Since 2009, certain locations within the study area, such as Karadikkuli, Kondachchi, and Silawatura, situated in close proximity to the Vilpattu forest buffer zone, have experienced encroachment by resettled individuals who have established residences and cultivated agricultural land.

Relationship between changing LST, NDVI, and ECI

While the deforestation rate hasn't been alarmingly high over the past 34 years, its ongoing pace has still considerably harmed forest health and environmental conditions. Moreover, there's a noticeable upward trend in this degradation. The distribution of LST is closely associated with the distribution of NDVI, suggesting a strong inverse correlation between LST and NDVI for the years 1988, 1996, and 2009, with an upward trajectory. *Jaafar et al. (2020)* reported analogous findings in their research conducted in Perak and Kedah, Malaysia. They also uncovered a robust correlation between LULC and LST. In this study, it was noted that as the NDVI values increase, the LST decreases. *Ranagalage, Estoque & Murayama (2017)* and *Dissanayake et al. (2019)* have both demonstrated that the expansion of built-up areas and barren lands contributes to an elevation in LST. Our research findings suggest a notable impact on ECI when LST rises. This is evident as the majority of areas exhibiting high LST also correspond to areas with high ECI in the study area. The regression analysis unveiled a consistently robust positive correlation between ECI and LST across all four time points, as evidenced by the R^2 values ranging from 0.8607 to 0.9640 (Fig. S4). In contrast to this pattern, the results revealed a significant inverse relationship between ECI and NDVI, with reported R^2 values ranging from 0.4029 to 0.8421.

Recommendation and future research direction

Deforestation emerges as a critical issue throughout the Mannar district, as evidenced by previous research conducted by *Rajendran (2019)*, *Luxmini et al. (2020)*, *Ranagalage et al. (2020)*, and *Fernando & Edirisuriya (2016)*. However, our study was confined to the Musali DSD due to constraints in resources and time. However, it is imperative to monitor alterations in forest cover and vegetation quality in other areas in the district, like Madu DSD, employing high-resolution remote sensing data. Since most dry zone districts like Vavuniya, Mullaitivu, Jaffna and Kilinochchi were resettled following the civil war after 2009, studies on LULC change and deforestation analysis become increasingly important for making decisions related to the conservation of dry evergreen forests in those regions.

This is attributed to a notable surge in resettlement and infrastructure development in those areas rapidly. Additionally, it is advisable to conduct a comparative study of various classification methods, such as support vector machine, k-mean algorithm, random forest, LandTrendr change detection algorithm, and neural networks, as demonstrated by *Dissanayake et al. (2019)*, *Rathnayake, Jones & Soto-Berelov (2020)* in future research endeavors. This could enhance accuracy and aid in selecting the most reliable method for analysis. Although our study did not exclude water bodies and vegetation areas in ECI calculation, it is recommended to exclude them to obtain more reliable results, following similar approaches as those adopted in studies by *Senanayake, Welivitiya & Nadeeka (2013)*, *Ranagalage, Estoque & Murayama (2017)*, and *Saputra, Jamadi & Sari (2023)*. VCI, is a widely utilized drought index for assessing vegetation drought stress. However, it may not be ideal for evaluating long-term trends in drought impacts on vegetation as emphasized by *Yin et al. (2024)* since VCI can inadvertently inherit the greening trend observed in NDVI. Therefore, it is advisable to conduct comparison studies on multi-source indicators of vegetation greenness and drought. Specifically, focusing on indices like Leaf Area Index (LAI), Palmer Drought Severity Index (PDSI), and Standardized Precipitation-Evapotranspiration Index (SPEI) as proposed by *Yin et al. (2024)*. Given the inherent limitations of Landsat data in NDVI calculation, it is advisable to explore alternative methods and datasets, such as deep learning-based approaches and Synthetic Aperture Radar (SAR) data as highlighted by *Malik, Shukla & Mishra (2019)*.

CONCLUSIONS

In our study, we endeavored to assess the dynamics in forest cover, vegetation health, and environmental conditions in Musali DSD utilizing Landsat time series data. The results obtained through supervised classification reveal a relatively moderate pace of deforestation spanning 34 years, with a total forest cover loss of 8.52 km^2 primarily linked to the expansion of settlements and paddy fields. The conversion had a significant impact on the health of the vegetation in the area, as indicated by a notable decline in NDVI and a subsequent rise in LST. Vegetation stress has escalated due to the increasing environmental vulnerability, particularly in deforested areas over the past two decades. The findings suggest a noteworthy impact on ECI growth across the four time periods due to the rise in LST. The regression analysis revealed that the degradation of vegetation conditions contributed to the increase in ECI. Given time and resource limitations, the study exclusively concentrated on Musali DSD. The reliability of our LULC findings is influenced by the inherent drawbacks of the MLC algorithm, such as its vulnerability to the distribution of categories in feature space and the sampling selection. Additionally, calculating NDVI using Landsat data encounters challenges arising from atmospheric conditions, sunlight and cloud cover. These factors limit the efficacy of multispectral bands in accurately capturing land characteristics. Moreover, NDVI is constrained by its capacity to solely capture linear relationships between NIR and red spectral bands, thereby limiting its ability to account for higher-order relationships between spectral channels. Because, VCI might unintentionally incorporate the prolonged greening pattern detected in NDVI, it could potentially compromise the reliability of our results.

ACKNOWLEDGEMENTS

The authors express gratitude to the anonymous reviewers and editors for their valuable comments provided on improving the quality of the manuscript. The authors are grateful to the U.S. Geological Survey (USGS) for providing open source Landsat data relevant to the study.

ADDITIONAL INFORMATION AND DECLARATIONS

Funding

This work was supported by the Researchers Supporting Project number (RSP2024R351), King Saud University, Riyadh, Saudi Arabia (financial support for APC of this article). The funders contributed to the conceptualization, data analysis, preparation of the manuscript. The funders did not have a role in data collection or decision to publish.

Grant Disclosures

The following grant information was disclosed by the authors:
Researchers Supporting Project number (RSP2024R351), King Saud University, Riyadh, Saudi Arabia.

Competing Interests

The authors declare there are no competing interests.

Author Contributions

- Neel Chaminda Withanage conceived and designed the experiments, performed the experiments, analyzed the data, prepared figures and/or tables, authored or reviewed drafts of the article, and approved the final draft.
- Prabuddh Kumar Mishra conceived and designed the experiments, analyzed the data, prepared figures and/or tables, and approved the final draft.
- Kamal Abdelrahman performed the experiments, authored or reviewed drafts of the article, and approved the final draft.
- Rajender Singh performed the experiments, authored or reviewed drafts of the article, and approved the final draft.

Data Availability

The following information was supplied regarding data availability:

The raw data and additional tables and figures are available in the Supplemental File.

Supplemental Information

Supplemental information for this article can be found online at http://dx.doi.org/10.7717/peerj.17714#supplemental-information.

REFERENCES

Alawamy JS, Balasundram SK, Hanif AMH, Sung CTB. 2020. Detecting and analyzing land use and land cover changes in the region of Al-Jabal Al-Akhdar, Libya using time-series landsat data from 1985 to 2017. *Sustainability* **12(11)**:4490 DOI 10.3390/su12114490.

Alqurashi AF, Kumar L. 2014. Land use and land cover change detection in the Saudi Arabian desert cities of Makkah and Al-Taif using satellite data. *Advanced Remote Sensing* **3**:106–119 DOI 10.4236/ars.2014.33009.

Anbazhagan S, Paramasivam CR. 2016. Statistical correlation between land surface temperature (LST) and vegetation index (NDVI) using multi-temporal landsat TM data. *International Journal of Earth Sciences and Engineering* **5**:333–346 DOI 10.23953/cloud.ijaese.204.

Athauda S, Wang Y, Hao Z, Indika S, Yapabandara I, Weragoda SK, Liu J, Wei Y. 2024. Geochemical assessment of the evolution of groundwater under the impact of seawater intrusion in the Mannar district of Sri Lanka. *Water* **16**:1137 DOI 10.3390/w16081137.

Culf AD, Esteves JL, Filho AOM, Da Rocha HR. 1996. Radiation, temperature and humidity over forest and pasture in Amazonia. In: *Amazonian Deforestation and Climate*. Chichester: John Wiley & Sons, 175–192.

Deng Y, Wang S, Bai X, Tian Y, Wu L, Xiao J, Chen F, Qian Q. 2018. Relationship among land surface temperature and LUCC, NDVI in typical karst area. *Scientific Reports* **8(1)**:641 DOI 10.1038/s41598-017-19088-x.

Department of Census and Statistics. 2022. *District statistical handbook*. Colombo: Department of Census and Statistics, Colombo, Sri Lanka.

Dissanayake D, Morimoto T, Ranagalage M, Murayama Y. 2019. Land-use/land-cover changes and their impact on surface urban heat islands: case study of Kandy City, Sri Lanka. *Climate* **7(8)**:99 DOI 10.3390/cli7080099.

Dutta D, Kundu A, Patel N, Saha S, Siddiqui A. 2015. Assessment of agricultural drought in Rajasthan (India) using remote sensing derived vegetation condition index (VCI) and standardized precipitation index (SPI). *Egyptian Journal of Remote Sensing and Space Sciences* **18**:53–63.

Estoque RC, Murayama Y. 2017. Monitoring surface urban heat island formation in a tropical mountain city using Landsat data (1987–2015). *ISPRS Journal of Photogrammetry and Remote Sensing* **133**:18–29 DOI 10.1016/j.isprsjprs.2017.09.008.

FAO. 2014. Global forest land-use change 1990–2010. An update to FAO forestry paper (169) the food and agricultural organization of the united nations (FAO) with the E.U. joint research centre (JRC). Rome: FAO.

FAO. 2022. The State of the World's Forests 2022. Forest pathways for green recovery and building inclusive, resilient and sustainable economies. Rome: FAO.

Fernández-Alonso FJ, Hernández Z, Torres-Costa V. 2023. A cost-effective portable multiband spectrophotometer for precision agriculture. *Agriculture* **13**:1467 DOI 10.3390/agriculture13081467.

Fernando GMTS, Edirisuriya CH. 2016. Identification of forest cover changes in Polonnaruwa District of Sri Lanka. In: *Proceedings of the 37th Asian conference remote sensing (ACRS 2016), Colombo, Sri Lanka.17–21 2016; Volume 1*. 224–228.

Fernando S, Senaratna A, Pallewatta N, Lokupitiya E, Manawadu L, Imbulana U, De Silva I, Ranwala S. 2015. Assessment of key policies and measures report on drivers of deforestation and forest degradation in Sri Lanka. Colombo: UN-REDD Programme.

Forest Department Government of Sri Lanka. 2009. Working paper no. APFSOS II/WP/2009/19 PAPUA New Guinea forestry outlook study. Bangkok, Sri Lanka: Forest Department Government of Sri Lanka.

Ha TV, Uereyen S, Kuenzer C. 2023. Agricultural drought conditions over mainland Southeast Asia: spatiotemporal characteristics revealed from MODIS-based vegetation time-series. *International Journal of Applied Earth Observation and Geoinformation* **121**:103378 DOI 10.1016/j.jag.2023.103378.

Jaafar WS, Abdul Maulud KN, Muhmad Kamarulzaman AM, Raihan A, Sah SMd, Ahmad A, Saad SNM, Mohd Azmi AT, Jusoh Syukri NKA, Razzaq Khan W. 2020. The Influence of Deforestation on Land Surface Temperature—A Case Study of Perak and Kedah, Malaysia. *Forests* **11(6)**:670 DOI 10.3390/f11060670.

Jenerette GD, Harlan SL, Brazel A, Jones N, Larsen L, Stefanov WL. 2006. Regional relationships between surface temperature, vegetation, and human settlement in a rapidly urbanizing ecosystem. *Landscape Ecology* **22**:353–365 DOI 10.1007/s10980-006-9032-z.

Kayet N, Pathak K. 2015. Remote sensing and GIS based land use/land cover change detection mapping in Saranda forest, Jharkhand, India. *International Research Journal of Earth Sciences* **3(1)**:2321–2527.

Kitić G, Tagarakis A, Cselyuszka N, Panić M, Birgermajer S, Sakulski D, Matović J. 2019. A new low-cost portable multispectral optical device for precise plant status assessment. *Computers and Electronics in Agriculture* **162**:300–308 DOI 10.1016/j.compag.2019.04.021.

Koellner T, Sell J, Gähwiler M, Scholz RW. 2008. Assessment of the management of organizations supplying ecosystem services from tropical forests. *Global Environmental Change* **18**:746–757 DOI 10.1016/j.gloenvcha.2008.07.009.

Kogan FN. 1990. Remote sensing of weather impacts on vegetation in non-homogeneous areas. *International Journal of Remote Sensing* **11**:1405–1419 DOI 10.1080/01431169008955102.

Land Use Policy Planning Department. 2016. Land use plan Mannar district. Colombo: Ministry of lands, Sri Lanka.

Luxmini KPAMK, Kishoran S, Sivanantharajah S, Gunatilake J. 2020. Identification of forest cover variation in Mannar district, Sri Lanka using GIS and remote sensing techniques. *International Journal of Applied Science and Technology* **5(2)**:69–77.

Malik MS, Shukla JP, Mishra S. 2019. Relationship of LST, NDBI and NDVI using landsat-8 data in kandaihimmat watershed, Hoshangabad, India. *Indian Journal of Geo-Marine Sciences* **48**:25–31.

Mohajane M, Essahlaoui A, Oudija F, Mohammed EH, Abdellah EH, Abdelhadi EO, Randazzo G, Teodoro AC. 2018. Land use/land cover (LULC) using landsat data series (MSS, TM, ETM+ and OLI) in Azrou Forest, in the Central Middle Atlas of Morocco. *Environments* **5(12)**:1–16 DOI 10.20448/journal.505.2018.51.1.7.

Olofsson P, Foody GM, Herold M, Stehman SV, Woodcock CE, Wulder MA. 2014. Good practices for estimating area and assessing the accuracy of land change. *Remote Sensing of the Environment* **148**:42–57 DOI 10.1016/j.rse.2014.02.015.

Padilla FM, Gallardo M, Peña Fleitas MT, De Souza R, Thompson RB. 2018. Proximal optical sensors for nitrogen management of vegetable crops: a review. *Sensors* **18(7)**:2083 DOI 10.3390/s18072083.

Peng S, Piao S, Zeng Z, Ciais P, Zhou L, Li L, Myneni R, Yin Y, Zeng H. 2014. Afforestation in China cools local land surface temperature. *Proceedings of the National Academy of Sciences of the United States of America* **111(8)**:2915–2919 DOI 10.1073/pnas.1315126111.

Rajendran N. 2019. An assessment of drought in Mannar district, Sri Lanka. *International Journal of Humanities and Applied Social* **4(11)**:1–13 DOI 10.33642/ijhass.v4n11p1.

Ranagalage M, Gunarthna MHJP, Surasinghe TD, Dissanayake D, Simwanda M, Murayama Y, Morimoto T, Phiri D, Nyirenda VR, Premakantha KT, Satharasinghe A. 2020. Multi-decadal forest-cover dynamics in the tropical realm: past trends and policy insights for forest conservation in dry zone of Sri Lanka forests. *Forest* **11(8)**:836 DOI 10.3390/f11080836.

Ranagalage M, Estoque RC, Murayama Y. 2017. An urban heat island study of the Colombo Metropolitan Area, Sri Lanka, based on Landsat data (1997–2017). *ISPRS International Journal of Geo-Information* **6(7)**:189 DOI 10.3390/ijgi6070189.

Rathnayake CW, Jones S, Soto-Berelov M. 2020. Mapping land cover change over a 25-year period (1993–2018) in Sri Lanka using landsat time-series. *Land* **9(1)**:1–19.

Rawat JS, Kumar M. 2015. Monitoring land use/cover change using remote sensing and GIS techniques: a case study of Hawalbagh block, district Almora, Uttarakhand, India. *The Egyptian Journal of Remote Sensing and Space* **18**:77–84.

Saputra LIA, Jamadi , Sari DN. 2023. Analysis of environmental criticality index (ECI) and distribution of slums in yogyakarta and surrounding areas using multitemporal landsat imagery. In: *Proceedings of the international conference of geography and disaster management (ICGDM 2022)*. Dordrecht: Atlantis Press, 407–420 DOI 10.2991/978-2-38476-066-4_26.

Senanayake IP, Welivitiya WDDP, Nadeeka PM. 2013. Remote sensing based analysis of urban heat islands with vegetation cover in Colombo city, Sri Lanka using Landsat-7 ETM+ data. *Urban Climate* **5**:19–35 DOI 10.1016/j.uclim.2013.07.004.

Sobrino JA, Jiménez-Muñoz JC, Paolini L. 2004. Land surface temperature retrieval from landsat TM 5. *Remote Sensing of the Environment* **90**:434–440 DOI 10.1016/j.rse.2004.02.003.

United State Geological survey. 2023. Earth explorer Landsat images. 1988, 1996, 2009 and, 2022. (public domain). *Available at https://earthexplorer.usgs.gov/*.

Weng Q. 2002. Land use change analysis in the Zhujiang Delta of China using satellite remote sensing, GIS and stochastic modelling. *Journal of Environmental Management* **64**:273–284 DOI 10.1006/jema.2001.0509.

Wickramagamage P. 1998. Large-scale deforestation for plantation agriculture in the hill country of Sri Lanka and its impacts. *Hydrological Processes* **12**:2015–2028 DOI 10.1002/(SICI)1099-1085(19981030)12:13/14<2015::AID-HYP716>3.0.CO;2-3.

Wijesinghe WMDC, Withanage WKNC. 2021. Detection of the changes in land use and land cover using remote sensing and GIS in Thalawa DS Division. *Prathimana Journal* **14**:72–86.

Withanage WKNC, Mishra PK, Jayasinghe BC. 2024. An assessment of spatio-temporal land use/land cover dynamics using landsat time series data (2008-2022) in Kuliyapitiya West Divisional secretariat division in Kurunagala district, Sri Lanka. *Journal of Geospatial Surveying* **4(1)**:12–23 DOI 10.4038/jgs.v4i1.52.

Wu C, Murray AT. 2003. Estimating impervious surface distribution by spectral mixture analysis. *Remote Sensing of the Environment* **84**:493–505 DOI 10.1016/S0034-4257(02)00136-0.

Yin G, He W, Liu X, Xia Y, Zhang H. 2024. Wetting or greening? Probing the global trends in vegetation condition index (VCI). *International Journal of Applied Earth Observation and Geoinformation* **129**:1–11.

Yuan X, Wang W, Cui J, Meng F, Kurban A, De Maeyer P. 2017. Vegetation changes and land surface feedbacks drive shifts in local temperatures over Central Asia. *Scientific Reports* **7**:3287 DOI 10.1038/s41598-017-03432-2.

Yuh YGW, Tracz H, Matthews D, Turner SE. 2023. Application of machine learning approaches for land cover monitoring in northern Cameroon. *Information Ecology* **74**:101955 DOI 10.1016/j.ecoinf.2022.101955.